NSG-7500 Preprint

APPLICATION OF PHOTOMETRIC MODELS TO ASTEROIDS

A 11A
11B GRANT
7N-91-CR
252404
46P.

Edward Bowell[1]

Bruce Hapke[2]

Kari Lumme[3]

Alan W. Harris[4]

Deborah Domingue[2]

and

Jouni Peltoniemi[3]

[1]Lowell Observatory, 1400 West Mars Hill Road, Flagstaff, Arizona 86001

[2]Department of Geology and Planetary Science, University of Pittsburgh, Pittsburgh, Pennsylvania 15260

[3]Observatory and Astrophysical Laboratory, University of Helsinki, Tähtitorninmäki, 00130 Helsinki, Finland

[4]Jet Propulsion Laboratory, 4800 Oak Grove Drive, Pasadena, California 91109

Submitted to *Asteroids II* 13 September 1988

Manuscript totals 46 pages, including 11 figures and 5 tables.

(NASA-CR-186151) APPLICATION OF PHOTOMETRIC MODELS TO ASTEROIDS (JPL) 46 p

N90-70562

Unclas

00/91 0252404

RUNNING HEAD: PHOTOMETRIC MODELS

ADDRESS FOR CORRESPONDENCE:

Dr. Edward Bowell
Lowell Observatory
1400 West Mars Hill Road
Flagstaff, Arizona 86001

ABSTRACT

The way an asteroid or other atmosphereless solar system body varies in brightness in response to changing illumination and viewing geometry depends in a very complicated way on the physical and optical properties of its surface and on its overall shape. We summarize the formulation and application of recent photometric models by Hapke and by Lumme and Bowell. In both models, the brightness of a rough and porous surface is parametrized in terms of the optical properties of individual particles, by shadowing between particles, and by the way in which light is scattered among collections of particles. Both models succeed in their goal of fitting the observed photometric behavior of a wide variety of bodies, but neither has led to a very complete understanding of the properties of asteroid regoliths, in part because of the restricted nature of groundbased photometric observations, but also because the parameters in the present models cannot be adequately constrained by observations of integral brightness alone.

1. INTRODUCTION

Since the last Tucson asteroids conference (Gehrels 1979), several models of light scattering in particulate surfaces, which are applicable to asteroids and other atmosphereless bodies, have been developed or refined. It is our purpose in this paper to summarize and compare results from two such models: by Hapke and by Lumme and Bowell. In particular, we have collected all the principal formulae together in one place, so that recipes for fitting photometric data, both disk-resolved and disk-integrated, are readily available to interested readers. First, however, it will be useful to sketch some of the progress that has been made during the last decade.

The photometric model developed by Hapke has been described in Hapke (1981, 1984, 1986) and Hapke and Wells (1981). It is assumed that geometric optics is valid. The contribution from singly scattered rays is derived exactly. The opposition effect is assumed to be due to hiding of the shadow of one particle on another and is derived by an approximation to the Seeliger-Irvine formulation (Irvine 1966), with significant differences that allow for a distribution of particle sizes and also include a more rigorous derivation of the extinction, scattering and absorption coefficients (Hapke 1986). The multiple-scattering contribution is calculated from a modified two-stream solution of the radiative transfer equation for isotropic scatterers and with a collimated source, which results in an analytic approximation to the Chandrasekhar H-functions.

Lumme and Bowell's model, given in its first form by Lumme and Bowell (1981a; hereafter LBa) also assumes geometric optics to be valid. Single and multiple components of light scattered in particulate surfaces are treated separately. In single scattering, a number of phase functions, due specifically to single particles, shadowing, and roughness, are combined; whereas multiple scattering is calculated using an approximate theory developed by Lumme and Reitsema (1978). In LBa, it was concluded that the opposition effect was controlled by porosity. However, in the present paper, recent work by Muinonen *et al.* (1988) on backscattering by

crystalline particles is invoked to explain what Lumme *et al.* (1987) have termed an *opposition spike*, apparent at phase angles smaller than a degree or two and present mainly in the phase curves of icy satellites. Such an explanation for sharp opposition spikes was apparently first proposed by Trowbridge (1978). Working along similar lines and following Morozhenko and Yanovitsky (1971), Shkuratov (1983) has imputed what he calls an optical concentration of light toward the source; he includes the effects of focussing, glory, and interference.

Both Hapke's and Lumme and Bowell's work have spawned applications, too numerous to detail here, aimed at fitting and interpreting photometric data on solar system bodies and laboratory samples. Discussions by Helfenstein and Veverka (1987) and Helfenstein (1988) give good summaries of work using Hapke's model on Mercury and the Moon (Hapke 1984, Buratti 1985, Veverka *et al.* 1988), Jovian and Saturnian satellites (Buratti 1983 and 1985, Helfenstein 1986, Simonelli and Veverka 1987), Uranian satellites and rings (Smith *et al.* 1986, Hapke 1986), and laboratory samples (Goguen 1981, Hapke and Wells 1981, Johnson *et al.* 1983, Mustard and Pieters 1987, Clark *et al.* 1988). Domingue and Hapke (1988) and Helfenstein and Veverka (1988) have used Hapke's model to fit asteroid phase curves. Lumme and Bowell's model was first applied to asteroids in a preliminary way by Bowell and Lumme (1979), and then more fully to a variety of atmosphereless bodies by Lumme and Bowell (1981b). Further work on asteroids has concerned pole and shape determination (Poutanen *et al.* 1981, Lumme *et al.* 1986, Magnusson *et al.* 1988), the effects of shape and albedo features on lightcurves and phase curves (Karttunen 1988, Karttunen and Bowell 1988), and the derivation of a two-parameter system for calculating magnitudes (Marsden 1986, Bowell *et al.* 1989). Other applications have been to the Moon (Lumme and Irvine 1982), Phobos and Deimos (Pang *et al.* 1983b), Jovian and Saturnian satellites (Lockwood *et al.* 1980a, 1980b, Pang *et al.* 1981, Pang *et al.* 1983a), the zodiacal cloud (Lumme and Bowell 1985), and laboratory samples (Lumme *et al.* 1980).

In the following two sections, we outline Hapke's and Lumme and Bowell's

photometric models. On the whole, we have chosen to adhere to the nomenclature and notation used in the original publications of the models, and have accordingly separately defined all the quantities used in each section. Although this has led to some repetition and some slightly different terminology for a few parameters, it has allowed each of the two treatments to be internally complete and consistent. In Section 4, we present fits to a selection of disk-resolved and disk-integrated data. Then, in Section 5, we compare and contrast the two models, and finally give some thoughts on possible future developments.

2. HAPKE'S PHOTOMETRIC MODEL

2.1. Photometric Relations for a Smooth Surface

The reflectances are functions of the angle of incidence i, the angle of emergence (viewing angle) e, the phase angle α, and the azimuth angle between the planes of incidence and emergence φ. These are related by

$$\begin{cases} \cos\alpha = \mu_0\mu + \sin i \sin e \cos\varphi \\ \mu_0 = \cos i \\ \mu = \cos e. \end{cases} \tag{1}$$

What is termed the *bidirectional reflectance* r is given by

$$r(i,e,\alpha) = \frac{w}{4\pi}\frac{\mu_0}{\mu_0+\mu}\{[1+B(\alpha)]p(\alpha) + H(\mu_0)H(\mu) - 1\}, \tag{2}$$

in which w is the average single-scattering albedo, $B(\alpha)$ is the opposition effect function, $p(\alpha)$ is the average single-particle scattering function, and H is an analytical approximation to Chandrasekhar's H-function for isotropic scatterers (cf. Eq. (7)).

For a mixture of particles of albedos w_i, densities ρ_i, diameters D_i, and mass fractions M_i,

$$w = (\sum_i M_i w_i/\rho_i D_i)/(\sum_i M_i/\rho_i D_i). \tag{3}$$

Thus the reflectance of a mixture may be calculated from the reflectances of the end members. The opposition effect function is

$$\begin{cases} B(\alpha) = B_0/[1 + \tan(\alpha/2)/h] \\ h = n\dfrac{\ln P^{-1}}{1-P} < \sigma >< r > \\ < r > = \sqrt{< \sigma > /\pi}. \end{cases} \tag{4}$$

Here, h is the angular width of the opposition effect, n is the number of particles per unit volume, P is the porosity, and $< \sigma >$ is the average extinction cross-section weighted by number. B_0 is the amplitude of the opposition effect. If the opposition effect is due only to the hiding of shadows between regolith particles, then $B_0 \leq 1$, and B_0 is the fraction of $wp(0)$ scattered from the portion of a particle surface that faces the source. However, individual particles can also be rough, composite, or behave like corner reflectors, and can thereby contribute to the opposition effect; this is taken into account by allowing B_0 to exceed unity. (Rigorously, another term of the same form as $B(\alpha)$ multiplying $p(\alpha)$ is required, but that would introduce two more parameters. Hence, $B(\alpha)$ should be interpreted as a composite opposition effect that may involve both the soil porosity and individual particle complexity.) The single-particle scattering function $p(\alpha)$ is empirically expressed either as an N-term Legendre polynomial expansion,

$$p(\alpha) = 1 + \sum_{n=1}^{N-1} a_n P_n(\alpha), \tag{5}$$

where a_n are constants and $P_n(\alpha)$ is the Legendre polynomial of degree n, or by a Henyey-Greenstein function of the form

$$p(\alpha) = (1 - b^2)/(1 - 2b\cos\alpha + b^2)^{3/2}, \tag{6}$$

as convenient. Usually, two or three terms suffice in the Legendre expansion. Since diffraction is not appropriate for particles in intimate contact, $p(\alpha)$ does not include

a diffraction term. Finally,

$$\begin{cases} H(x) = (1+2x)/(1+2\gamma x) \\ \gamma = \sqrt{1-w}. \end{cases} \tag{7}$$

Note that H is a function of both angle and single-scattering albedo.

The so-called *bihemispherical reflectance* r_0 is calculated from

$$r_0 = (1-\gamma)/(1+\gamma). \tag{8}$$

The *directional-hemispherical reflectance* for a two-term $p(\alpha)$ of the form

$$p(\alpha) = 1 + a\cos\alpha \tag{9}$$

is given by

$$A_H(i) = r_0 \frac{1+\gamma}{1+2\gamma\mu_0} + a\frac{w}{4}\frac{\mu_0}{1+\mu_0}. \tag{10}$$

For a spherical planet of uniform albedo, with $p(\alpha)$ given by Eq. (9), the *Bond albedo* for a two-term $p(\alpha)$ is

$$A_B = r_0\left[1 - \frac{1}{3}\frac{\gamma}{1+\gamma} + 0.69a(1+\gamma)^2\right]; \tag{11}$$

the *physical* or *geometric albedo* is

$$A_P = (w/8)[(1+B_0)p(0) - 1] + (r_0/2 + r_0^2/6); \tag{12}$$

and the *integral phase function* is given by

$$\begin{aligned} \Phi(\alpha) = (1/A_P)\Big\{ &\Big[(w/8)[(1+B(\alpha))p(\alpha) - 1] \\ &+ (r_0/2)(1-r_0)\Big]\Big[1 - \sin(\alpha/2)\tan(\alpha/2)\ln[\cot(\alpha/4)]\Big] \\ &+ (2r_0^2/3\pi)[\sin\alpha + (\pi-\alpha)\cos\alpha]\Big\}. \end{aligned} \tag{13}$$

2.2. Photometric Relations for a Rough Surface

The derivation of the photometric functions of a macroscopically rough surface takes into account two major effects: (1) *Shadows*: One part of the surface can prevent another part from being illuminated or from being seen by the detector. (2) *Effective surface tilt*: Portions of the surface tilted away from the source or detector have a greater probability of not being illuminated or seen than portions of the surface tilted toward the source or detector, resulting in the average surface being tilted toward the source and detector.

It is assumed in the model that the surface is made up of unresolved facets tilted at various angles. The angles of tilt are assumed to be distributed uniformly in azimuth and described by a function $A(\theta)$, where θ is the angle between the normal to the facet and the normal to the mean surface. In Hapke (1984), $A(\theta)$ was assumed to be given by a Gaussian distribution in $\tan\theta$. The sizes of the facets are large compared to the extinction mean free path $1/n\sigma$, but small compared to the detector footprint on the surface of the body. Double and higher-order reflections between facets are ignored. However, multiple scattering between grains of soil within each facet is included.

The roughness is described by a characteristic slope angle $\overline{\theta}$, defined by

$$\tan\overline{\theta} = (2/\pi)\int_0^{\pi/2} \tan\theta A(\theta)d\theta. \tag{14}$$

Shadowing is described by a shadow function $S(i,e,\alpha)$ and surface tilt by replacing μ and μ_0 by effective cosines μ_e and μ_{oe}, respectively.

The *bidirectional reflectance of a rough surface* is given by

$$r(i,e,\alpha) = \frac{w}{4\pi}\frac{\mu_{oe}}{\mu_{oe}+\mu_e}\{[1+B(\alpha)]p(\alpha) + H(\mu_{oe})H(\mu_e) - 1\}S(i,e,\varphi). \tag{15}$$

Let

$$\begin{cases} f(\varphi) = e^{-2\tan(\varphi/2)} \\ C(\overline{\theta}) = (1+\pi\tan\overline{\theta})^{-1/2} \\ E_1(x) = e^{-(2/\pi)\cot\overline{\theta}\cot x} \\ E_2(x) = e^{-(1/\pi)\cot^2\overline{\theta}\cot^2 x}. \end{cases} \tag{16}$$

Then S, μ_e, and μ_{oe} have slightly different forms depending on the relative values of i and e.

If $i \leq e$:

$$\begin{cases} \mu_{oe}(i,e,\varphi) = C(\overline{\theta})\Big[\mu_0 + \sin i \tan\overline{\theta}\ \dfrac{\cos\varphi E_2(e) + \sin^2(\varphi/2)E_2(i)}{2 - E_1(e) - (\varphi/\pi)E_1(i)}\Big] \\ \mu_e(i,e,\varphi) = C(\overline{\theta})\Big[\mu + \sin e \tan\overline{\theta}\ \dfrac{E_2(e) - \sin^2(\varphi/2)E_2(i)}{2 - E_1(e) - (\varphi/\pi)E_1(i)}\Big] \\ S(i,e,\varphi) = \dfrac{\mu_e(i,e,\varphi)}{\mu_e(0,e,0)}\dfrac{\mu_0}{\mu_{oe}(i,0,\pi)}C\overline{\theta})\Big\{1 - f(\varphi)\big[1 - C(\overline{\theta})\dfrac{\mu_0}{\mu_{oe}(i,0,\pi)}\big]\Big\}^{-1}. \end{cases} \tag{17}$$

If $i \geq e$:

$$\begin{cases} \mu_{oe}(i,e,\varphi) = C(\overline{\theta})\Big[\mu_0 + \sin i \tan\overline{\theta}\ \dfrac{E_2(i) - \sin^2(\varphi/2)E_2(e)}{2 - E_1(i) - (\varphi/\pi)E_1(e)}\Big] \\ \mu_e(i,e,\varphi) = C(\overline{\theta})\Big[\mu + \sin e \tan\overline{\theta}\ \dfrac{\cos\varphi E_2(i) + \sin^2(\varphi/\pi)E_2(e)}{2 - E_1(i) - (\varphi/\pi)E_1(e)}\Big] \\ S(i,e,\varphi) = \dfrac{\mu_e(i,e,\varphi)}{\mu_e(0,e,\pi)}\dfrac{\mu_0}{\mu_{oe}(i,0,0)}C(\overline{\theta})\Big\{1 - f(\varphi)\big[1 - C(\overline{\theta})\dfrac{\mu}{\mu_e(0,e,\pi)}\big]\Big\}^{-1}. \end{cases} \tag{18}$$

The *physical albedo of a rough surface* is given by

$$A_P = (w/8)[(1+B_0)p(0) - 1] + (r_0/2 + r_0^2/6)C(w,\overline{\theta}), \tag{19}$$

where

$$C(w,\overline{\theta}) = 1 - (0.048\overline{\theta} + 0.0041\overline{\theta}^{\,2})r_0 - (0.33\overline{\theta} - 0.0049\overline{\theta}^{\,2})r_0^2. \tag{20}$$

And the *integral phase function of a spherical body with a rough surface* is derived from

$$\begin{aligned}\Phi(\alpha) = &\left\{(w/8)[(1+B_0)p(0)-1]+r_0/2+r_0^2/6\right\}^{-1} \\ &\times\Big\{\big[(w/8)[(1+B(\alpha))p(\alpha)-1] \\ &+(r_0/2)(1-r_0)\big]\big[1-\sin(\alpha/2)\tan(\alpha/2)\ln[\cot(\alpha/4)]\big] \\ &+(2r_0^2/3\pi)[\sin\alpha+(\pi-\alpha)\cos\alpha]\Big\}K(\alpha,\overline{\theta}),\end{aligned} \tag{21}$$

where $K(\alpha,\overline{\theta})$ is given in Table I. For $\alpha < 60°$, an analytical approximation is

$$K(\alpha,\overline{\theta}) \approx e^{-[0.32\sqrt{\tan\overline{\theta}\tan(\alpha/2)}+0.52\tan\overline{\theta}\tan(\alpha/2)]\overline{\theta}}, \tag{22}$$

3. LUMME AND BOWELL'S PHOTOMETRIC MODEL

3.1. Disk-Resolved Brightness

In their original work (LBa), Lumme and Bowell gave the reflection coefficient πr in the form

$$\frac{I}{F} \equiv \pi r = \pi r_1 + \pi r_m, \tag{23}$$

where πF is the incident flux, πI the emergent flux, πr_1 the contribution from single scattering, and πr_m that from multiple scattering. Explicitly,

$$\begin{cases} \pi r_1 = \dfrac{\varpi_0}{2}P(\alpha)\Phi_S(\alpha,\lambda)\dfrac{\mu_0}{\mu+\mu_0}\left(\dfrac{\sigma}{1+\rho\xi}+1-\sigma\right) \\ \pi r_m = \dfrac{\varpi_0^*}{4}\left[h(\mu,\varpi_0^*)h(\mu_0,\varpi_0^*)-1\right], \end{cases} \tag{24}$$

where ϖ_0 is the single-scattering albedo, ϖ_0^* is the single-scattering albedo according to the "similarity relations" approximation, P is the single-particle phase function, Φ_S is the mutual shadowing function (normalized to unity at $\alpha = 0°$, as all Φs have

been in the following), σ is the fraction of the surface covered with "holes" (called q in LBa; σ is used here to avoid confusion with the symbol conventionally used for the phase integral), ρ is a measure of the surface roughness (roughly, the tangent of the mean surface slope at the millimeter scale), and h is a multiple-scattering function (approximated by Chandrasekhar's H function). In addition,

$$\begin{cases} \xi = \dfrac{\sqrt{\mu^2 + \mu_0^2 - 2\mu\mu_0 \cos\alpha}}{\mu\mu_0} \equiv \dfrac{\sin\alpha}{\cos\beta\cos\lambda\cos(\lambda - \alpha)} \\ \mu = \cos\beta\cos\lambda \\ \mu_0 = \cos\beta\cos(\lambda - \alpha), \end{cases} \tag{25}$$

where β is the photometric latitude and λ the longitude. The shadowing function is given by the expression

$$\begin{cases} \Phi_S(y) = ye^y \displaystyle\int_0^1 x^{2y-1} e^{-xy} dx \equiv \frac{1}{2} {}_1F_1(1, 1 + 2y; y) \\ y = \dfrac{\ln \frac{1}{1-D}}{2.4} \dfrac{\cos\lambda + \cos(\lambda - \alpha)}{\sin\alpha}, \end{cases} \tag{26}$$

in which ${}_1F_1$ is a degenerate hypergeometric function and D is the volume density of the regolith, here assumed constant with depth. Eqs. (23–26) summarize Lumme and Bowell's model for surface brightness.

Before studying the consequences and results of Lumme and Bowell's model, the following should be noted: (1) The singly scattered flux πr_1 does not tend to zero at the limb ($\mu \to 0$). (2) The principle of conservation of energy is not seriously violated: A straightforward check may be made by directly integrating I/F to yield the Bond albedo for the case of conservative scattering, i.e., $\varpi_0 = 1$, with the result that there is a slight underestimate. (3) The shadowing function Φ_S: After Eq. (17) (LBa), an approximation $\ln(1 - x) \approx -x$ is given and stated to be valid only for small volume densities, but if D is large, the correct expression, Eq. (26), should be used.

3.2. Single-Particle Phase Function

Both Hapke and Lumme and Bowell have used a physical model to parametrize most of the effects that play a role in light scattering by regoliths, with the exception of the single-particle phase function $P(\alpha)$. Appropriate specification of this function is essential for the interpretation of the integrated brightness data, which are also functions of the same variable. Even for disk-resolved data at a fixed $\alpha, P(\alpha)$ is important because it determines the absolute scale for single scattering, but only if there exist disk-resolved data at several widely separated phase angles can one hope to solve for $P(\alpha)$ independently. Hitherto, Lumme and Bowell have been using either isotropic scattering ($P \equiv 1$) or a single Henyey-Greenstein phase function, the latter of which is an analytical representation having no physical basis. Hapke has on occasion chosen to use a three-term Legendre expansion (having two free parameters), which also lacks physical justification.

To provide deeper insight into P, two further sources have been called upon: Microwave analog measurements made by Giese *et al.* (1978) on realistic non-spherical particles, and theoretical ray-tracing calculations for statistically rough particles by Peltoniemi *et al.* (1988). All four of the absorbing fluffy or rough particles measured by Giese *et al.* have refractive indices in the range $1.45 \leq n \leq 1.65$, and the imaginary part times the size parameter (a descriptor of absorption) on the order of unity, making them well suited for treatment of the photometry of low-albedo bodies (Mercury, for example). When properly normalized (the integral of P over 4π equals one) the measurements indicate that all four particles have small, roughly linear backward scattering for $0° \leq \alpha \leq 90°$, strong forward scattering for $\alpha \geq 120°$, and that P is similar for all particles. The data can be well represented (Fig. 1) by an empirical function, somewhat different from that used by Peltoniemi *et al.*, of the form

$$\begin{cases} P(\alpha) = Be^{-b\alpha} + Fe^{-f(\pi-\alpha)} \\ F = \dfrac{1+f^2}{1+e^{-\pi f}}\left[2 - \dfrac{B}{1+b^2}(1+e^{-\pi b})\right], \end{cases} \tag{27}$$

where the expression for F comes from normalization and

$$\begin{cases} B = P(0°) = 0.95 \\ F = P(180°) = 16.15 \\ b = 0.4 \text{ rad}^{-1} \\ f = 4.0 \text{ rad}^{-1}. \end{cases} \tag{28}$$

Diffraction is not included in this function. A two-term Henyey-Greenstein function does not give such a good fit, and a high-degree Legendre function would be required to provide an equally good fit. Equation (27) suggests that, in the backward regime,

$$P(\alpha) \approx B - Bb\alpha. \tag{29}$$

Using geometric optics, Peltoniemi *et al.* (1988) have theoretically studied light scattered by statistically deformed spheres. They assumed a log-normal distribution of the particle radius vector, and varied both the amount of deformation and the optical parameters. It is clear from their work that Eq. (27) is a good approximation, with values in the range of Eq. (28).

A recently discovered sharp opposition effect, here termed the *opposition spike*, has been observed in the phase curves of some high-albedo objects at very small phase angles. It has led to the addition here of another component to P. Obviously, single-particle scattering of the type characterized by Eq. (27) is suitable only for irregular particles. Ices and regolith-forming minerals can, however, exist in crystalline form. Some of these crystals have right-angle troughs, making them very effective backscatterers (retroreflectors). Muinonen *et al.* (1988) have calculated the light-scattering properties of a number of common crystal forms by using ray-tracing techniques, allowing the optical constants to vary. The resulting calculated phase curves can be well fitted in the important phase angle range $0.1° \leq \alpha \leq 10°$ by

$$P(\alpha) = Ae^{-\frac{\alpha}{0.333^{\alpha}+0.231\alpha}} \equiv A\Phi_c(\alpha), \tag{30}$$

where α in degrees. A more rigorous but more complicated approximation has been given by Muinonen *et al.* (1988). The unknown scale factor $A \geq 10$ results from the use of geometric optics, which breaks down at $\alpha = 0°$, where the rigorous theory of physical optics should be used (such a theory does not exist for non-spherical particles). Eqs. (27) and (30) can now be combined as a plausible mean single-particle phase function. If v stands for the fractional volume occupied by crystals and $1 - v$ that occupied by irregular particles then, for $\alpha \lesssim 100°$,

$$\begin{cases} P(\alpha) = vA\Phi_c(\alpha) + (1-v)Be^{-b\alpha} \\ \Phi_P(\alpha) = \dfrac{P(\alpha)}{P(0)} = c\Phi_c(\alpha) + (1-c)e^{-b\alpha} \\ c = \dfrac{va}{vA + (1-v)B}. \end{cases} \tag{31}$$

3.3. Disk-Integrated Brightness

The disk-integrated brightness of a spherical body of unit radius can be calculated from

$$L(\alpha) = \pi F \int_{-\pi/2}^{\pi/2} d\beta \cos^2\beta \int_{\alpha-\pi/2}^{\pi/2} r(\lambda, \beta, \alpha) \cos\lambda \, d\lambda \equiv \pi F R(\alpha). \tag{32}$$

The classical integrated descriptors of brightness can be conveniently expressed in terms of $R(\alpha)$:

$$\begin{cases} p = \dfrac{L(0°)}{\frac{1}{\pi}\pi^2 F} = R(0°) \\ q = 2\displaystyle\int_0^{\pi} \frac{R(\alpha)}{R(0°)} \sin\alpha \, d\alpha \\ A = pq = 2\displaystyle\int_0^{\pi} R(\alpha) \sin\alpha \, d\alpha. \end{cases} \tag{33}$$

It might be a good policy to refer to $R(\alpha)$ as the *pseudoalbedo* of a body at fixed phase angle α lest there be confusion with the geometric albedo p.

Equation (32) can be transformed into the form

$$
\left\{
\begin{aligned}
\Phi_{obs}(\alpha) &= (1-Q)\Phi_1(\alpha) + Q\Phi_M(\alpha) \\
\Phi_1 &= \Phi_P[\sigma\Phi_R + (1-\sigma)\Phi_0] \\
\Phi_0 &= \Phi_R(\rho = 0) \\
\Phi_R &= \frac{1}{2\cos\frac{1}{2}\alpha}\int_0^{\frac{1}{2}(\pi-\alpha)} \frac{(2\cos^2\varphi - z_0)^2}{2\cos^2\varphi - z_1}\,\frac{y_0 + \cos\varphi}{2y_0 + \cos\varphi}\,\frac{d\varphi}{\cos\varphi} \\
\Phi_M &= \frac{R_M(\alpha)}{R_M(0°)} \\
R_M(\alpha) &= \frac{\varpi_0^*}{2\pi}\int_0^{\pi/2} d\beta\cos^2\beta \int_{\alpha-\pi/2}^{\pi/2} \left[h(\cos\beta\cos\lambda)h(\cos\beta\cos(\lambda-\alpha)) - 1\right] \\
&\qquad \times \frac{\cos\lambda\cos(\lambda-\alpha)}{\cos\lambda + \cos(\lambda-\alpha)}d\lambda \\
y_0 &= \frac{1.8}{\ln\frac{1}{1-D}}\sin\alpha/2 \\
z_0 &= 1 - \cos\alpha \\
z_1 &= z_0 - \frac{\rho}{0.6}\sin\alpha,
\end{aligned}
\right.
\tag{34}
$$

where Φ_P is given by Eq. (31). In deriving the expression for Φ_R, two approximations have been used:

$$
\left\{
\begin{aligned}
\int_0^{\pi/2} \frac{\cos^3\beta\, d\beta}{z + \cos\beta} &\approx \frac{\pi/4}{1 + 1.2z} \\
\Phi_S(y) &\approx \frac{y + 3/4}{y + 3/2},
\end{aligned}
\right.
\tag{35}
$$

both of which are accurate at the 1% level.

Since Φ_1 and Φ_M are not known, Φ_1 and Φ_2 as defined by Bowell *et al.* (1989) are adopted, as follows:

$$\begin{cases} \Phi_i = W\Phi_{iS} + (1-W)\Phi_{iL}; \quad i = 1,2 \\ W = \exp(-90.56\tan^2\tfrac{1}{2}\alpha) \\ \Phi_{iS} = 1 - \frac{C_i \sin\alpha}{0.119+1.341\sin\alpha - 0.754\sin^2\alpha} \\ \Phi_{iL} = \exp\left[-A_i(\tan\tfrac{1}{2}\alpha)^{B_i}\right] \\ A_1 = 3.332 \qquad A_2 = 1.862 \\ B_1 = 0.631 \qquad B_2 = 1.218 \\ C_1 = 0.986 \qquad C_2 = 0.238. \end{cases} \tag{36}$$

For Φ_1, the best nonlinear least-squares solution was sought with the four parameters b, D, ρ, and σ. Because the opposition spike was not manifestly present in the data set used by Bowell *et al.*, it is natural to set c [cf. Eq. (31)] equal to zero. However, properly determined h-functions are not yet available to explain the empirical function Φ_2 (or Φ_M), which is in any case somewhat steeper than would be derived from classical radiative transfer theory. This matter is currently under investigation. Solution values for the parameters in Φ_1 are

$$\begin{cases} b = 0.21 \text{ rad}^{-1} \\ D = 0.24 \\ \rho = 1.34 \\ \sigma = 1.00, \end{cases} \tag{37}$$

for which the rms (relative) error is 1.3%. It must be emphasized that the solution, Eq. (37), is not unique, except for D, and that a strong correlation exists between parameters. To see this explicitly, b and σ can be constrained to be consistent with the Mercury disk-resolved data ($b = 0.38$ rad^{-1}, $\sigma = 0.71$; cf. Section 4.1). Whence, solving only for D and ρ, one obtains

$$\begin{cases} D = 0.22 \pm 0.04 \\ \rho = 1.7 \pm 0.3, \end{cases} \tag{38}$$

with a slightly larger rms.

To explain the opposition-spike data, the effect of crystals is taken into account by rewriting Eq. (34) in three-parameter form:

$$\begin{cases} 10^{-0.4V_{obs}(\alpha)} = a_1\Phi_1(\alpha) + a_2\Phi_2(\alpha) + bF_c(\alpha) \\ F_c = \Phi_1\Phi_c \\ a_1 = (1-c)(1-Q)10^{-0.4H} \\ a_2 = Q10^{-0.4H} \\ b = c(1-Q)10^{-0.4H}, \end{cases} \tag{39}$$

where V_{obs} is a reduced observed magnitude, Φ_1 and Φ_2 are given by Eq. (36), Φ_c is given by Eq. (30), and $H \equiv V(0°)$.

4. MODEL FITS TO SELECTED PHOTOMETRIC DATA

Often the integral phase curve of an asteroid is known only for a small range of phase angles: $\alpha < 25°$, say. Over this restricted portion of the phase curve, some of the parameters in both Hapke's and Lumme and Bowell's formulations have similar effects on $\Phi(\alpha)$, and it is usually very difficult to disentangle them. Hence, *a unique interpretation of the phase curve in terms of the physical properties of the asteroid is usually not possible from the integral phase curve alone.* Furthermore, it is not possible to obtain the single-scattering albedo, which determines the ratio of multiply to singly scattered radiation, from the integral phase curve alone, although the single-scattering albedo can sometimes be constrained by measurements of the geometric albedo.

However, if the integral phase curve is known over a wide range of phase angles (from less than 2° to greater than 90°, say) and if the geometric albedo is known, then it is sometimes possible to obtain a unique fit and physical interpretation. If disk-resolved data are available over a wide range of phase angles, then it is possible to separate these effects and thereby obtain unique values of the photometric parameters and to interpret them in terms of physical properties of the surface.

4.1. Disk-Resolved Data

Disk-resolved photometry of Mercury has been taken from Mariner 10 orange-filter image FDS 2577. It consists of radiances observed at $\alpha = 77°$ and normalized to those of a Lambert surface illuminated vertically and observed at zero phase angle. In Fig. 2, the data have been fitted using Hapke's model with parameter values as given in Table IV.

To model the Mercury data using Lumme and Bowell's formulation, Eq. (24) is written in the following form, noting that $\Phi_S = 0.5$, since $\alpha \gg 0°$:

$$\begin{cases} \pi r = a_1 f_1 + a_2 f_2 + f \\ a_1 = \dfrac{\varpi_0}{4} P(77°)\sigma \\ a_2 = \dfrac{\varpi_0}{4} P(77°)(1-\sigma) \\ f_1 = \dfrac{\mu_0}{\mu + \mu_0} \\ f_2 = \dfrac{f_1}{1+\rho\xi} \\ f = \dfrac{\varpi_0^*}{4} f_1 \left[h(\mu, \varpi_0^*) h(\mu_0, \varpi_0^*) - 1\right]. \end{cases} \tag{40}$$

Using the Mariner 10 data both for $\beta = 0°$ (photometric equator) and $\lambda = 50°$ (meridian), the free parameters a_1, a_2, ρ, and ϖ_0^* were calculated by nonlinear least squares, with the result that χ^2 was most sensitive to ϖ_0^*, thus imposing the constraint $0.44 \leq \varpi_0^* \leq 0.52$ by the 2-σ criterion. The dependence on ρ is relatively weak because both a_1 and a_2 are small quantities. From the derived values of a_1

and a_2, one can deduce that

$$\begin{cases} \frac{\varpi_0}{4} P(77°) = 0.051 \\ \sigma = 0.71 \\ 1.0 \leq \rho \leq 1.5. \end{cases} \tag{41}$$

As can be seen from Tables II and III and Fig. 3, the fits are good.

It is notable that, with no further information, one can solve only for σ, the fraction of the surface covered with "holes." If one accepts the value derived for the asymmetry factor g that results from the single-particle phase function suggested above: namely, $g = 0.04$, one can solve for ϖ_0 and $P(77°)$, obtaining $\varpi_0 = 0.46$ and $P(77°) = 0.44$, a result that is in remarkably good agreement with the value obtained by means of the phase function defined in Eq. (34). (Note that g alone does not constrain P, so a circular argument is not being invoked.) If the geometric albedo p and multiple-scattering factor Q (the ratio of multiply to singly scattered light at zero phase angle) of the body are also known, as is the case for Mercury (for which $p = 0.13$ and $Q = 0.23$), one can not only derive additional information but can also check some of the conclusions. Unfortunately, the integrated-brightness data for Mercury are very noisy, particularly when $\alpha \leq 20°$. Therefore, use has instead been made of the much less noisy data for the Moon (Rougier 1933), which are almost indistinguishable. Now

$$p_1 = (1 - Q)p = \frac{\varpi_0}{4} P(0°) = 0.10 \tag{42}$$

and

$$p_M = Qp = \frac{\varpi_0}{4} \int_0^1 [H^2(\mu, \varpi_0) - 1]\mu \, d\mu = 0.03, \tag{43}$$

where p_1 is the geometric albedo of a single particle and p_M is the multiple-scattering contribution to the geometric albedo. From Eq. (42), one can calculate that $P(0°) =$

0.89, which agrees remarkably well with the value of B above. Inserting $\varpi_0 = 0.46$ in Eq. (44), one finds that $p_M = 0.024$, a value that is certainly within the observational error of p.

Although it is true that, by analyzing the disk-resolved brightness, disk-integrated brightness, and microwave analog measurements, an internally consistent picture of Mercury's light-scattering properties has been arrived at using Lumme and Bowell's model, a caveat is in order: Disk-resolved photometry is available at only one phase angle, and use has been made of several approximations for the true radiative transfer process in a rough regolith made up of closely packed particles. This situation, of course, violates the requirements of classical radiative transfer theory and, therefore, the corrections for multiple scattering could be prone to error.

4.2. Disk-Integrated Data

An integral phase curve of Mercury derives from Danjon (1949), and is constrained to have a geometric albedo of 0.14. A comparison of Hapke's model with the data is given in Fig. 4a; a three-term Legendre expansion was used for $p(\alpha)$. Because of the noisiness of Danjon's data, Lumme and Bowell have chosen to fit whole disk photometry of the Moon, as mentioned above; the fit is shown in Fig. 4b.

Phase-curve data for asteroids derive from the following sources: 24 Themis, pertaining to brightness averaged over rotation (Harris *et al.* 1989a); 44 Nysa, mean brightness (Harris *et al.* 1989b); 69 Hesperia, brightness at primary maximum (Poutanen *et al.* 1985); 82 Alkmene, maximum brightness (Harris *et al.* 1984b); 133 Cyrene, maximum brightness (Harris *et al.* 1984a); 419 Aurelia, mean brightness (Harris and Young 1989); and 1862 Apollo, maximum brightness (Harris *et al.* 1987).

For the integral phase curves of the asteroids, the Henyey-Greenstein expression for $p(\alpha)$ given by Eq. (6) was used. Then $\Phi(\alpha)$ contains five parameters: w, B_0, h, b and $\overline{\theta}$. Examples of fits of the model to observed photometric data on various bodies are shown in Figs. 5a through 11a. The fits were made by trial-and-error variation of the five parameters. Parameter values for the fitted curves are given in Table IV. In

almost all cases, the goodness of fit is consistent with the quality of the observations. An exception, however, is 1862 Apollo, whose phase curve was most likely distorted both by large changes in the amplitude and shape of the lightcurve with increasing phase angle and by changes in aspect angle during the long intervals spanned by the observations.

In Lumme and Bowell (1981b), there was discussion of the indeterminacy of model parameters, in particular the roughness ρ and the asymmetry factor g. It was found, however, that mean values of the volume density D and surface roughness sufficed to represent the entire dataset of 74 asteroid phase curves, all of which could be well fitted by varying only the multiple-scattering factor Q. In accordance with the rather similar findings given in Section 3.3 of this paper, and adding the quantity c to parametrize the opposition spike, least-squares fits of Eq. (39) were made to the asteroid datasets (in the relative sense, to give equal weight in magnitude space). Fitted phase curves are also shown in Figs. 5b through 11b, and the resulting values of H, Q, and c, together with the rms magnitude residuals, are given in Table V.

Most of the fits are very good, and are comparable with those from Hapke's model, as can be seen from values of the rms residuals in Tables IV and V. Only in the case of 419 Aurelia's phase curve, which has a markedly less pronounced opposition effect than those of the other bodies considered, is there a systematic run of magnitude residuals that indicates a slight failure of Lumme and Bowell's model, at least in the three-parameter form used here. In Hapke's model, Aurelia's small opposition effect is accounted for by a small value of B_0 and a large value of b (cf. Table IV). However, in Lumme and Bowell's model, an improvement can be made by increasing the volume density D. From the values of c one cannot uniquely determine the fractional volume of crystals v, Eq. (31), because geometric optics does not provide a means of estimating the brightness of a crystal at $\alpha = 0°$. However, a crude estimate *can* be made because one can be almost certain that $A \geq 10$ when $v \leq c/(10 - 9c)$ (Muinonen *et al.* 1988). This implies that an admixture of just a few percent of material in the form of crystals could explain the observed opposition spike.

5. COMPARISON, CONTRAST, AND FUTURE WORK

Although the mathematical formalisms of the two models are somewhat different, both rest on similar assumptions. The major difference is in the treatment of roughness. In Lumme and Bowell's model, roughness affects only the single-scattering terms, thus implicitly assuming that the major contribution to shadowing occurs on scales on the order of that of the extinction length—a few particle diameters. In Hapke's model, by contrast, roughness affects both the single- and multiple-scattering terms, thus assuming that shadowing is important on all scales. Lumme and Bowell's model overestimates the brightness for surfaces of low albedo, and is most nearly exact for high-albedo surfaces; whereas Hapke's model is more correct for surfaces of low albedo, and underestimates the brightness for high-albedo surfaces.

In both Hapke's model and Lumme and Bowell's model, it is agreed that the classical opposition effect at phase angles $2° \lesssim \alpha \lesssim 7°$ is caused by mutual shadowing. Hapke's model achieves a narrow opposition effect by taking account of the effects of particle size distribution and predicts lunar soil porosities consistent with those measured for Apollo samples (Hapke 1986). Lumme and Bowell's model leads to volume densities that are typical of those seen in particulate laboratory samples (Lumme *et al.* 1980).

Another difference between the two models as presented here is the parametrization of the newly discovered opposition spike. Hapke allows the amplitude of the opposition effect B_0 to exceed unity. Lumme and Bowell are convinced that the opposition spike is caused by the presence of crystalline particles, which act as retroreflectors. To account for the effect in their model, the single-particle phase function is modified.

In both models, the parameters in the mathematical expressions for the geometric albedo and integral phase function can be associated with physical properties of asteroid surfaces, such as porosity, roughness, and the light-scattering properties of individual soil particles. Thus, we may hope to obtain information about asteroid

surfaces from observations of the integral brightnesses. For instance, in the original formulation of Lumme and Bowell's model, the opposition effect was taken to be controlled by porosity and the linear part of the phase curve by roughness. Unfortunately, we now realize that, at the present state of development of the models (c. 1988), unique values of the parameters cannot be determined because different parameters may have similar effects on the phase curves (cf. Domingue and Hapke 1988; Helfenstein and Veverka 1988). Hence, the associated physical properties of asteroid surfaces cannot be assigned with any confidence. If the models are to be fully useful, a major task for the future will be to find ways of constraining the parameters that will allow unique fits to observational data.

Other important tasks for the future will be to generalize the classical radiative transfer theory to include the effects of (1) a statistically rough upper boundary instead of smooth, plane-parallel geometry; (2) the conditional propagation probability for a photon whose entire history is known (this becomes important in close packing); (3) a discrete, finite-sized, and closely packed medium, rather than the continuous medium required by classical theory. First steps towards solving these questions have been undertaken by Muinonen *et al.* (1988) and Peltoniemi *et al.* (1988).

ACKNOWLEDGMENTS

EB's funding derives from NASA Grant NSG–7500 and from the Lowell Observatory endowment. BH's and DD's research is supported by a grant from the Planetary Geology and Geophysics Program, Solar System Exploration Division, of NASA. AWH has been funded at the Jet Propulsion Laboratory under contract from NASA.

REFERENCES

Bowell, E., A. W. Harris, and K. Lumme (1989). A two-parameter magnitude system for asteroids. To be submitted to *Icarus*.

Bowell, E., and K. Lumme (1979). Colorimetry and magnitudes of asteroids. In *Asteroids* (T. Gehrels, Ed.), pp. 132–169. University of Arizona Press, Tucson.

Buratti, B. J. (1983). *Photometric Properties of Europa and the Icy Satellites of Saturn.* Ph.D. thesis, Cornell University, Ithaca, New York.

Buratti, B. J. (1985). Applications of a radiative transfer model to bright icy satellites. *Icarus* **61**, 208–217.

Clark, R. N., K. S. Kierein, and G. A. Swayes (1988). Experimental verification of the Hapke reflectance theory. 1. Computation of reflectance as a function of grain size and wavelength based on optical constants. In press.

Danjon, A. (1949). Photométrie et colorimétrie des planètes Mercure et Vénus. *Bull. Astron.* **14**, 315–345.

Domingue, D., and B. Hapke (1988). Fitting theoretical photometric functions to asteroid phase curves. Submitted to *Icarus.*

Gehrels, T. (1979). Editor, *Asteroids*, 1181 pp., University of Arizona Press, Tucson.

Giese, R. H., K. Weiss, R. H. Zerull, and T. Ono (1978). Large fluffy particles: A possible explanation of the optical properties of interplanetary dust. *Astron. Astrophys.* **65**, 265–272.

Goguen, J. (1981). *A Theoretical and Experimental Investigation of the Photometric Functions of Particulate Surfaces.* Ph.D. thesis, Cornell University, Ithaca, New York.

Hapke, B. (1981). Bidirectional reflectance spectroscopy. 1. Theory. *J. Geophys. Res.* **86**, 3039–3054.

Hapke, B. (1984). Bidirectional reflectance spectroscopy. 3. Correction for macroscopic roughness. *Icarus* **59**, 41–59.

Hapke, B. (1986). Bidirectional reflectance spectroscopy. 4. The extinction coefficient and the opposition effect. *Icarus* **67**, 264–280.

Hapke, B. and E. Wells (1981). Bidirectional reflectance spectroscopy. 2. Experiments and observations. *J. Geophys. Res.* **86**, 3055–3060.

Harris, A. W., M. Carlsson, J. W. Young, and C.-I. Lagerkvist (1984a). The

lightcurve and phase relation of the asteroid 133 Cyrene. *Icarus* **58**, 377–382.

Harris, A. W., J. W. Young, F. Scaltriti, and V. Zappalà (1984b). Lightcurves and phase relations of the asteroids 82 Alkmene and 444 Gyptis. *Icarus* **57**, 251–258.

Harris, A. W., J. W. Young, J. Goguen, H. B. Hammel, G. Hahn, E. Tedesco, and D. J. Tholen (1987). Photoelectric lightcurves of the asteroid 1862 Apollo. *Icarus* **70**, 246–256.

Harris, A. W., and J. W. Young (1989). Photoelectric lightcurves of asteroids: 1980 observations from Table Mountain Observatory. To be submitted to *Icarus*.

Harris, A. W., J. W. Young, E. Bowell, L. J. Martin, R. L. Millis, M. Poutanen, F. Scaltriti, V. Zappalà, H. J. Schober, H. Debehogne, and K. W. Zeigler (1989a). Photoelectric observations of asteroids 3, 24, 60, 261, and 863. *Icarus*, in press.

Harris, A. W., J. W. Young, and L. Contreiras (1989b). Paper reporting photometry of 44 Nysa and 64 Angelina. To be submitted to *Icarus*.

Helfenstein, P. (1986). *Derivation and Analysis of Geological Constraints on the Emplacement and Evolution of Terrains on Ganymede from Applied Differential Photometry.* Ph.D. thesis, Brown University, Providence, Rhode Island.

Helfenstein, P. (1988). The geological interpretation of photometric surface roughness. *Icarus* **73**, 462–481.

Helfenstein, P., and J. Veverka (1987). Photometric properties of lunar terrains derived from Hapke's equation. *Icarus* **72**, 342–357.

Helfenstein, P., and J. Veverka (1988). Physical properties of asteroid surfaces from photometric analysis. In Asteroids II (R. P. Binzel, T. Gehrels, and M. S. Matthews, Eds.), pp. xxx–xxx. University of Arizona Press, Tucson.

Irvine, W. (1966). The shadowing effect in diffuse reflectance. *J. Geophys. Res.* **71**, 2931–2937.

Karttunen, H. (1988). Modelling asteroid brightness variations. I. Numerical methods. *Astron. Astrophys.*, in press.

Karttunen, H., and E. Bowell (1988). Modelling asteroid brightness variations. II. On the uninterpretability of lightcurves and phase curves. *Astron. Astrophys.*,

in press.

Lockwood, G. W., K. Lumme, and D. T. Thompson (1980a). The recent photometric variability of Io. *Icarus* **44**, 240–248.

Lockwood, G. W., D. T. Thompson, and K. Lumme (1980b). A possible detection of solar variability: Photometry of Io, Europa, Callisto, and Rhea, 1976–1979. *Astron. J.* **85**, 961–968.

Lumme, K., and E. Bowell (1981a). Radiative transfer in the surfaces of atmosphereless bodies. I. Theory. *Astron. J.* **86**, 1694–1704.

Lumme, K., and E. Bowell (1981b). Radiative transfer in the surfaces of atmosphereless bodies. II. Interpretation of phase curves. *Astron. J.* **86**, 1705–1712.

Lumme, K., and E. Bowell (1985). Photometric properties of zodiacal light particles. *Icarus* **62**, 54–71.

Lumme, K., E. Bowell, and B. Zellner (1980). Interpretation of laboratory sample photometry by means of a generalized radiative transfer theory. *Lunar and Planetary Science XI*, pp. 637–639. Lunar and Planetary Institute, Houston.

Lumme, K., and Irvine, W. M. (1982). Radiative transfer in the surfaces of atmosphereless bodies. III. Interpretation of lunar photometry. *Astron. J.* **87**, 1076–1082.

Lumme, K., H. Karttunen, E. Bowell, and M. Poutanen (1986). Inversion of asteroid lightcurves using spherical harmonics. In *Asteroids, Comets, Meteors II* (C.–I. Lagerkvist, B. A. Lindblad, H. Lundstedt, and H. Rickman, Eds.), pp. 55–59. Uppsala University, Sweden.

Lumme, K., K. Muinonen, J. Peltoniemi, H. Karttunen, and E. Bowell (1987). A possible explanation for anomalously sharp opposition effects. *Bull. Am. Astron. Soc.* **19**, 850.

Lumme, K., and H. J. Reitsema (1978). Five-color photometry of Saturn and its rings. *Icarus* **33**, 288–300.

Magnusson, P., M. A. Barucci, J. D. Drummond, K. Lumme, S. J. Ostro, J. Surdej, R. C. Taylor, and V. Zappalà (1988). Determination of pole orientations and

shape parameters of asteroids. In Asteroids II (R. P. Binzel, T. Gehrels, and M. S. Matthews, Eds.), pp. xxx–xxx. University of Arizona Press, Tucson.

Marsden, B. G. (1986). Notes from the IAU General Assembly. *Minor Planet Circ.* Nos. 10193 and 10194.

Morozhenko, A. V., and E. G. Yanovitsky (1971). Optical properties of the surface layer of the Moon. *Astron. Zh.* **48**, 172–183.

Muinonen, K., K. Lumme, J. Peltoniemi, and W. M. Irvine (1988). Light scattering by randomly oriented crystals. Submitted to *Appl. Optics.*

Mustard, J. F., and C. M. Pieters (1987). Quantitative abundance estimates from bidirectional reflectance measurements. *Proc. Seventeenth Lunar Sci. Conf., Part 2, J. Geophys. Res.* **92**, E617–E626.

Pang, K. D., J. M. Ajello, K. Lumme, and E. Bowell (1983a). Interpretation of whole-disk photometry of Callisto and Ganymede. *J. Geophys. Res.* **88**, A569–A576.

Pang, K. D., K. Lumme, and E. Bowell (1981). Microstructure and particulate properties of the surfaces of Io and Ganymede: Comparison with other solar system bodies. *Proc. Lunar Plan. Sci. Conf.* **12B**, 1543–1553.

Pang, K. D., J. W. Rhoads, G. A. Hanover, K. Lumme, and E. Bowell (1983b). Interpretation of whole-disk photometry of Phobos and Deimos. *J. Geophys. Res.* **88**, 2475–2484.

Peltoniemi, J., K. Lumme, K. Muinonen, and W. M. Irvine (1988). Scattering of light by stochastically rough particles. Submitted to *Appl. Optics.*

Poutanen, M., E. Bowell, and K. Lumme (1981). A physically plausible ellipsoidal model of Hektor? *Bull. Am. Astron. Soc.* **13**, 725.

Poutanen, M., E. Bowell, L. J. Martin, and D. T. Thompson (1985). Photoelectric photometry of asteroid 69 Hesperia. *Astron. Astrophys. Suppl. Ser.* **61**, 291–297.

Rougier, G. (1933). Photométrie photoélectrique globale de la Lune. *Ann. Obs. Strasbourg* **2**, 205–339.

Shkuratov, Yu. G. (1983). Model of the Heiligenschein of atmosphereless cosmic bodies. *Astron. Zh.* **60**, 1005–1008.

Simonelli, D. P., and J. Veverka, J. (1987). Phase curves of materials on Io: Interpretation in terms of Hapke's function. *Icarus* **68**, 503–521.

Smith, B. A., L. A. Soderblom, R. Beebe, D. Bliss, J. M. Boyce, A. Brahic, G. A. Briggs, R. H. Brown, S. A. Collins, A. F. Cook II, S. K. Croft, J. N. Cuzzi, G. E. Danielson, M. E. Davies, T. E. Dowling, D. Godfrey, C. J. Hansen, C. Harris, G. E. Hunt, A. Ingersoll, T. V. Johnson, R. J. Krauss, H. Masursky, D. Morrison, T. Owen, J. B. Plescia, J. B. Pollack, C. C. Porco, K. Rages, C. Sagan, E. M. Shoemaker, L. A. Sromovsky, C. Stoker, R. G. Strom, V. E. Suomi, S. P. Synnott, R. J. Terrille, P. Thomas, W. R. Thompson, and J. Veverka (1986). Voyager 2 in the Uranian system: Imaging science results. *Science* **233**, 43–64.

Trowbridge, T. S. (1978). Retroreflection from rough surfaces. *J. Opt. Soc. Am.* **68**, 1225–1245.

Veverka, J., P. Helfenstein, B. Hapke, and J. Goguen (1988). Photometry and polarimetry of Mercury. In *Mercury* (C. R. Chapman, Ed.). University of Arizona Press, Tucson. In press.

TABLE I.
HAPKE'S INTEGRAL PHASE FUNCTION
ROUGHNESS CORRECTION FACTOR $K(\alpha, \overline{\theta})$

α	$\overline{\theta}$						
(°)	0°	10°	20°	30°	40°	50°	60°
0	1.00	1.00	1.00	1.00	1.00	1.00	1.00
2	1.00	0.997	0.991	0.984	0.974	0.961	0.943
5	1.00	0.994	0.981	0.965	0.944	0.918	0.881
10	1.00	0.991	0.970	0.943	0.909	0.866	0.809
20	1.00	0.988	0.957	0.914	0.861	0.797	0.715
30	1.00	0.986	0.947	0.892	0.825	0.744	0.644
40	1.00	0.984	0.938	0.871	0.789	0.692	0.577
50	1.00	0.982	0.926	0.846	0.748	0.635	0.509
60	1.00	0.979	0.911	0.814	0.698	0.570	0.438
70	1.00	0.974	0.891	0.772	0.637	0.499	0.366
80	1.00	0.968	0.864	0.719	0.566	0.423	0.296
90	1.00	0.959	0.827	0.654	0.487	0.346	0.231
100	1.00	0.946	0.777	0.575	0.403	0.273	0.175
110	1.00	0.926	0.708	0.484	0.320	0.208	0.130
120	1.00	0.894	0.617	0.386	0.243	0.153	0.094
130	1.00	0.840	0.503	0.290	0.175	0.107	0.064
140	1.00	0.747	0.374	0.201	0.117	0.070	0.041
150	1.00	0.590	0.244	0.123	0.069	0.040	0.023
160	1.00	0.366	0.127	0.060	0.032	0.018	0.010
170	1.00	0.128	0.037	0.016	0.0085	0.0047	0.0026
180	1.00	0	0	0	0	0	0

TABLE II.
LUMME–BOWELL MODEL:
FIT TO MARINER 10 DATA
ALONG MERCURY'S PHOTOMETRIC
EQUATOR ($\beta = 0°$)

$\lambda(°)$	πr_{obs}	πr_{calc}
80	0.050	0.047
60	0.046	0.047
40	0.038	0.038
20	0.025	0.026
0	0.011	0.011
5	0.007	0.006

TABLE III.
LUMME-BOWELL MODEL:
FIT TO MARINER 10 DATA
ALONG A MERIDIAN
OF MERCURY($\lambda = 50°$)

$\beta(°)$	πr_{obs}	πr_{calc}
0	0.044	0.043
20	0.041	0.041
40	0.037	0.038
60	0.030	0.030
70	0.023	0.024
75	0.018	0.021

TABLE IV.
HAPKE'S MODEL:
PARAMETERS FOR FITTED PHASE CURVES

Body	w	B_0	h	b	$\bar{\theta}$	rms Residual (mag)	Geometric Albedo
24 Themis	0.048	1.6	0.060	0.40	5°	0.011	0.061
44 Nysa	0.58	0.6	0.0055	0.40	27	0.014	0.492
69 Hesperia	0.154	0.94	0.036	0.40	35	0.017	0.147
82 Alkmene	0.183	1.4	0.047	0.28	5	0.017	0.138
133 Cyrene	0.204	1.19	0.022	0.383	10	0.012	0.21
419 Aurelia	0.204	0.47	0.030	0.60	25	0.011	0.044
1862 Apollo	0.28	0.98	0.026	0.325	2	0.042	0.21
Mercury[1]	0.21	1.85	0.030	0.40	20	0.12	0.14

[1]A three-term Legendre polynomial was used for $p(\alpha)$ [cf. Eq. (5)] with $c = 0.4$.

TABLE V.
LUMME-BOWELL MODEL:
CONSTRAINED($0 \leq c \leq 1$) LEAST-SQUARES FITS
TO PHASE-CURVE DATA

Body	H (mag)	Q	c	rms Residual (mag)
24 Themis	7.097	0.201	0.000	0.016
44 Nysa	6.844	0.522	0.311	0.024
69 Hesperia	7.054	0.240	0.026	0.013
82 Alkmene	7.778	0.201	0.469	0.013
133 Cyrene	7.763	0.254	0.252	0.007
419 Aurelia	8.438	0.170	0.000	0.028
1862 Apollo	16.232	0.225	0.000	0.050
Moon	−0.089	0.233	0.000	0.023

FIGURE CAPTIONS

Figure 1. The single-particle phase function $P(\alpha)$. Intensity (arbitrary units) is plotted as a function of scattering angle ($= 180° - \alpha$) for four nonspherical particles (Giese *et al.* 1978). The fitted curve is from Eq. (27).

Figure 2. Fits to disk-resolved photometry of Mercury using Hapke's model. (a) Reflectance as a function of longitude along the photometric equator. (b) Reflectance as a function of latitude along the meridian $\lambda = 50°$.

Figure 3. As Fig. 2, using Lumme and Bowell's model.

Figure 4. Fitted phase curves for (a) Mercury, using Hapke's model, and (b) the Moon, using Lumme and Bowell's model.

Figure 5. Fitted phase curves for 24 Themis, using (a) Hapke's model, and (b) Lumme and Bowell's model.

Figure 6. As Fig. 5, for 44 Nysa.

Figure 7. As Fig. 5, for 69 Hesperia.

Figure 8. As Fig. 5, for 82 Alkmene.

Figure 9. As Fig. 5, for 133 Cyrene.

Figure 10. As Fig. 5, for 419 Aurelia.

Figure 11. As Fig. 5, for 1862 Apollo.

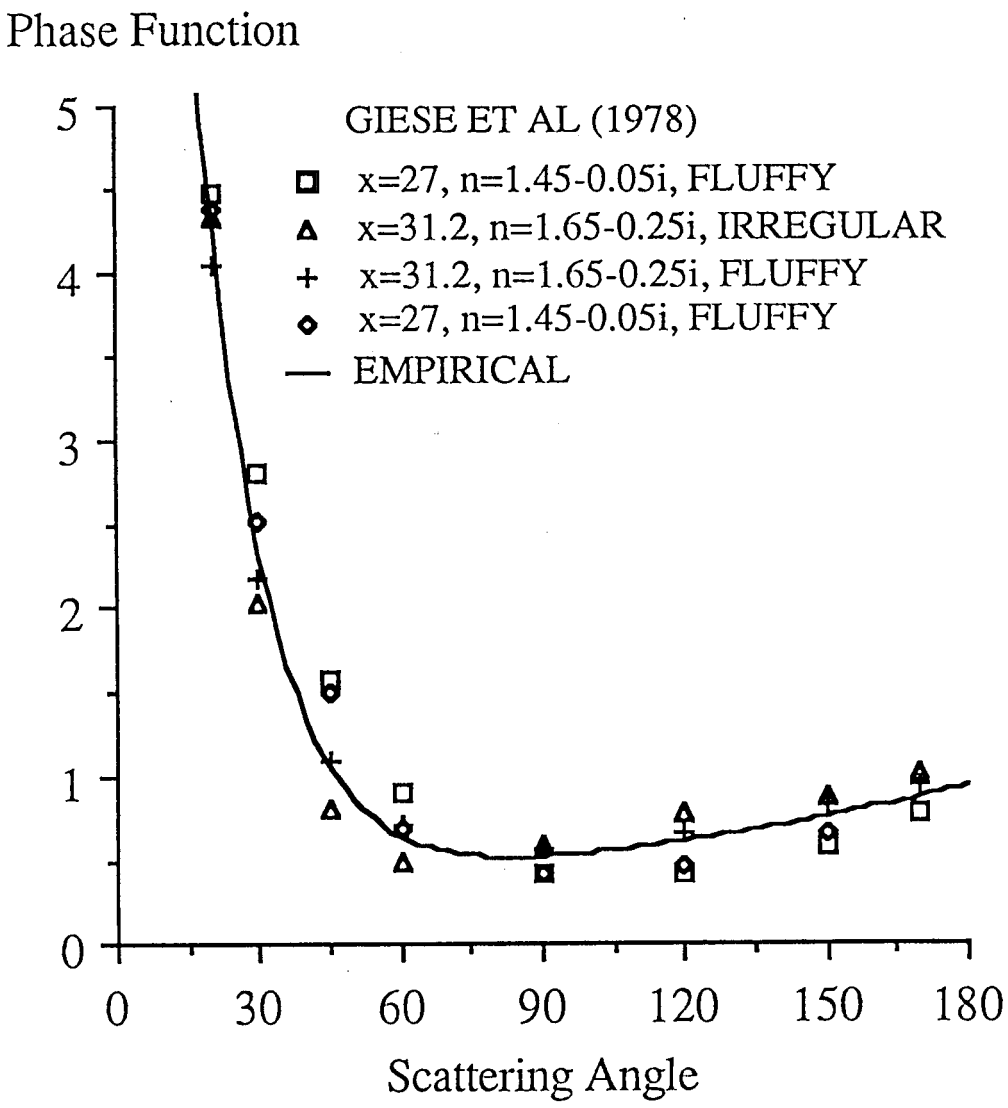
Phase Function
GIESE ET AL (1978)
x=27, n=1.45-0.05i, FLUFFY
x=31.2, n=1.65-0.25i, IRREGULAR
x=31.2, n=1.65-0.25i, FLUFFY
x=27, n=1.45-0.05i, FLUFFY
EMPIRICAL
5
4
3
2
1
0
0
30
60
90
120
150
180
Scattering Angle

Fig. 1

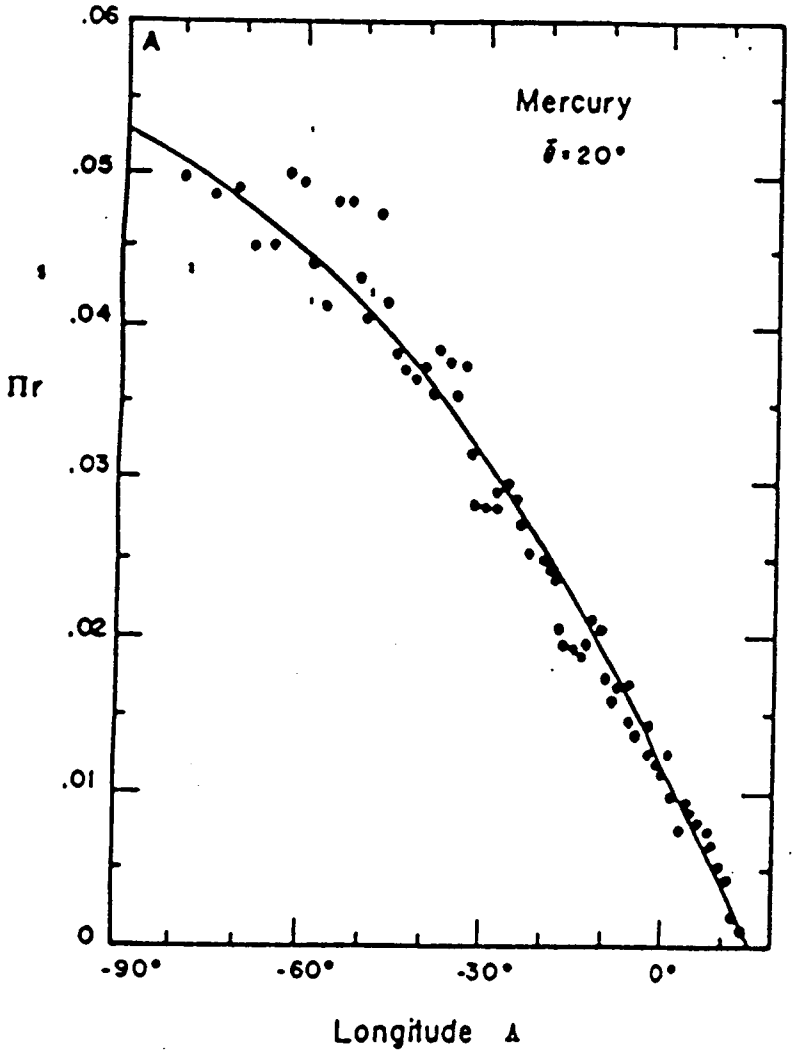
A
Mercury
δ = 20°
Πr
.06
.05
.04
.03
.02
.01
0
-90°
-60°
-30°
0°
Longitude Λ

Fig. 2a

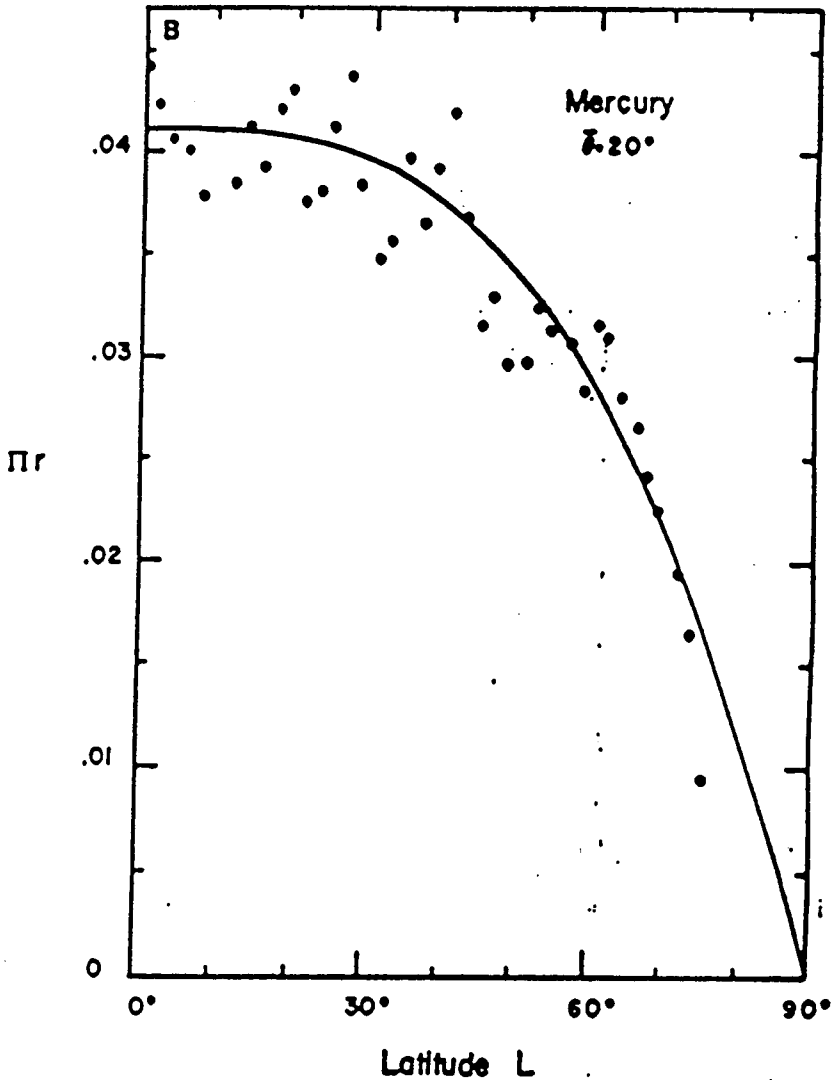
B
Mercury
δ = 20°
Πr
.04
.03
.02
.01
0
0°
30°
60°
90°
Latitude L

Fig. 2b

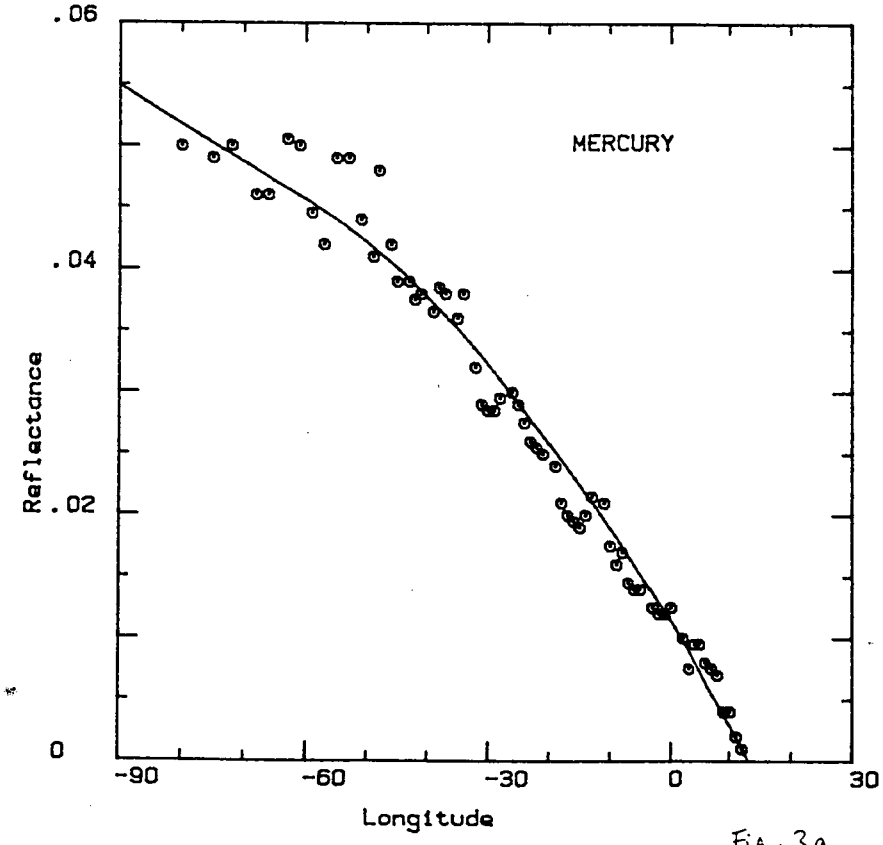
MERCURY
Reflectance
.06
.04
.02
0
-90
-60
-30
0
30
Longitude

Fig. 3a

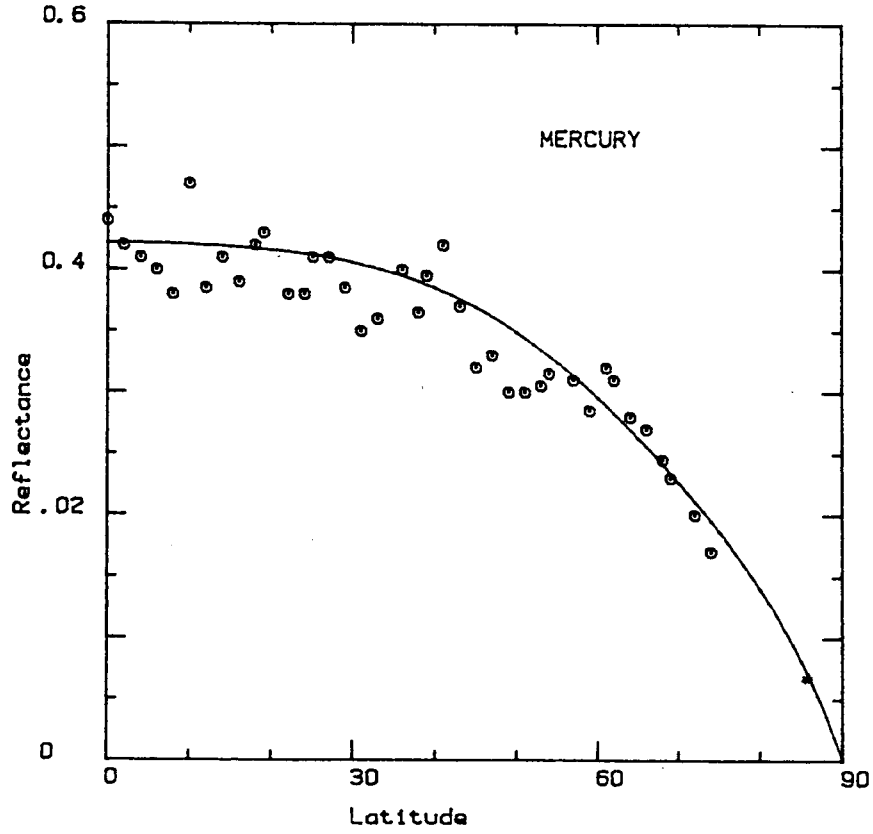
MERCURY
Reflectance
0.6
0.4
.02
0
0
30
60
90
Latitude

Fig. 3b

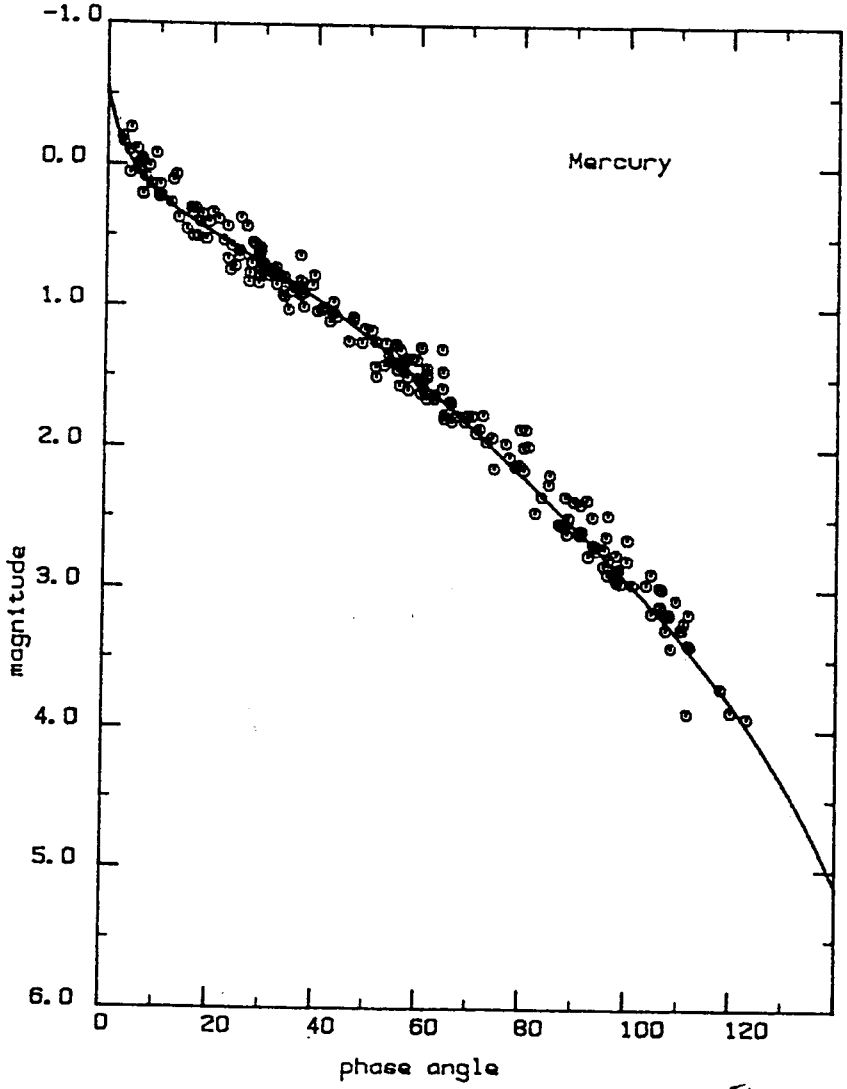
Mercury
magnitude
phase angle
-1.0
0.0
1.0
2.0
3.0
4.0
5.0
6.0
0
20
40
60
80
100
120

Fig. 4a

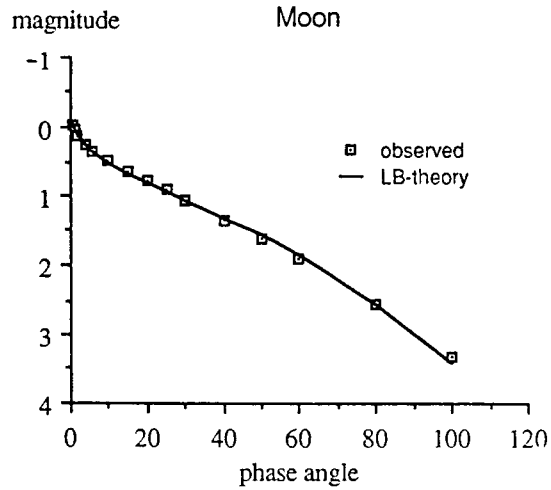
Moon
magnitude
observed
LB-theory
phase angle
-1
0
1
2
3
4
0
20
40
60
80
100
120

Fig. 4b

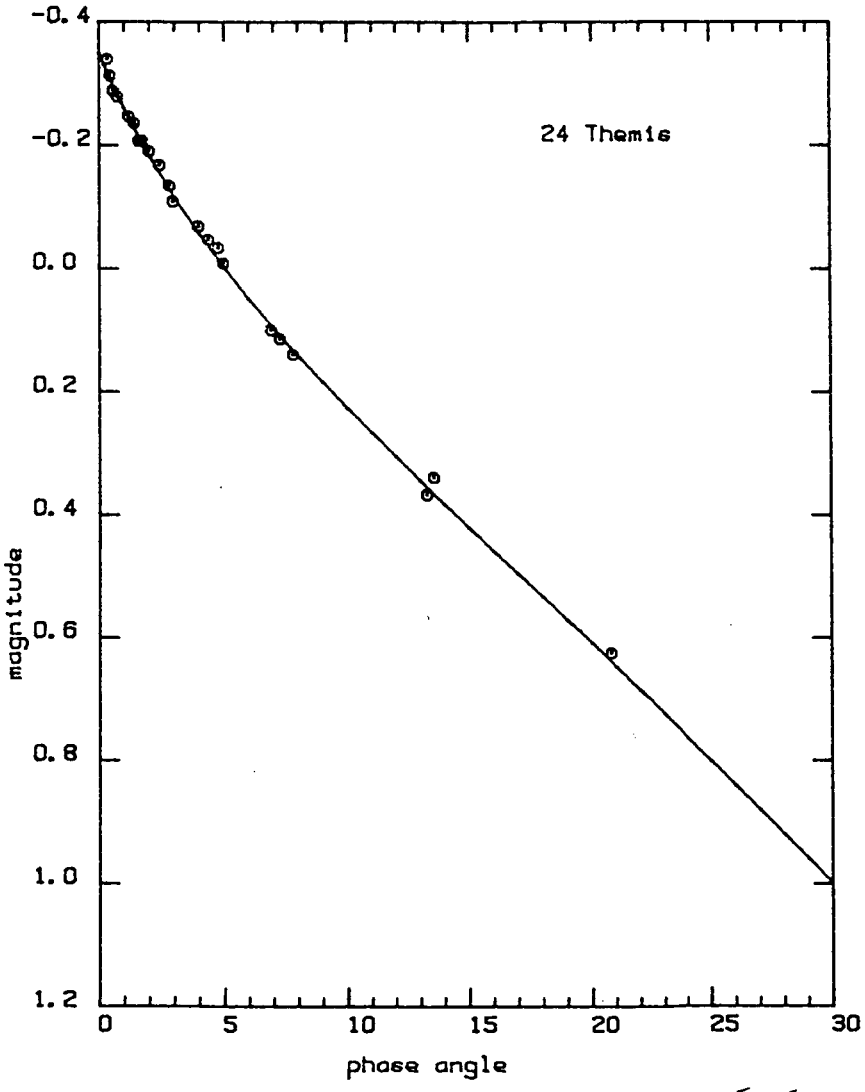
24 Themis
magnitude
phase angle
-0.4
-0.2
0.0
0.2
0.4
0.6
0.8
1.0
1.2
0
5
10
15
20
25
30

Fig. 5a

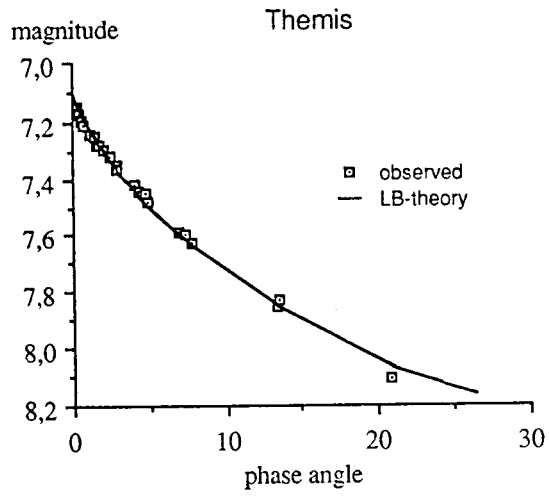
Themis
magnitude
observed
LB-theory
phase angle
7,0
7,2
7,4
7,6
7,8
8,0
8,2
0
10
20
30

Fig. 5b

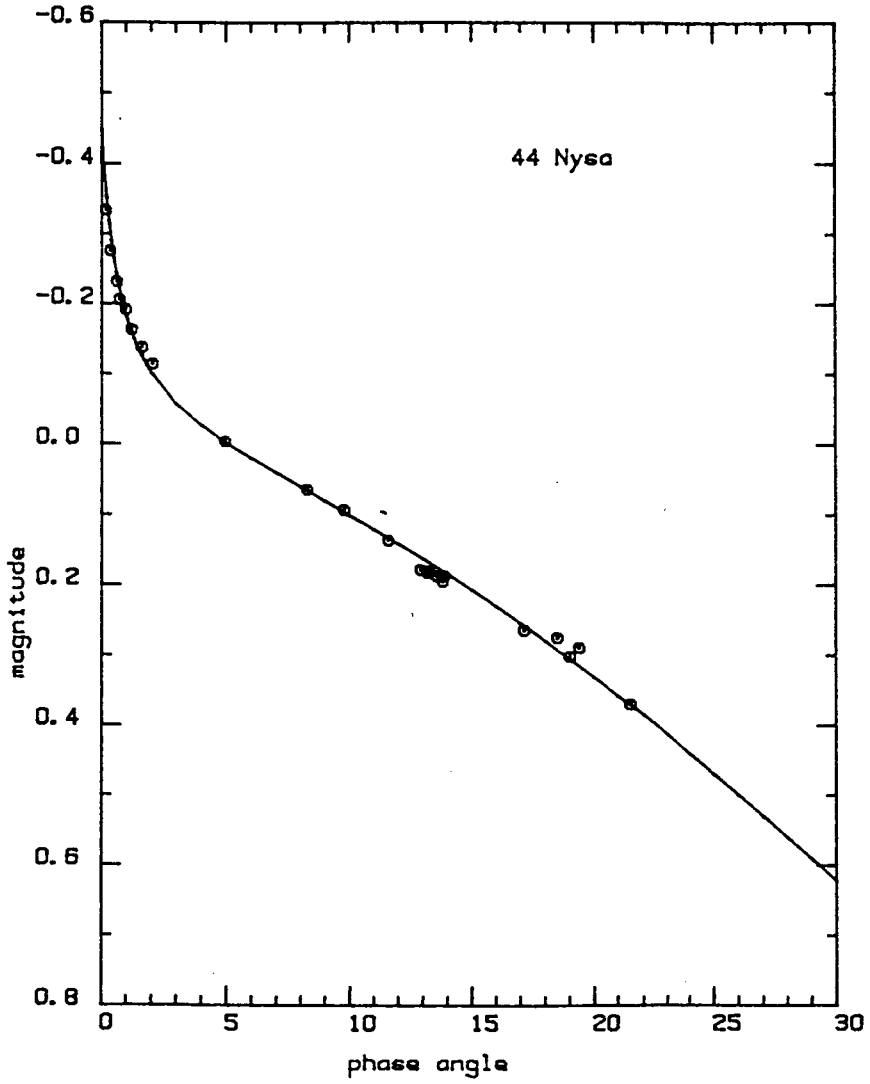
44 Nysa
magnitude
phase angle
-0.6
-0.4
-0.2
0.0
0.2
0.4
0.6
0.8
0
5
10
15
20
25
30

Fig. 6a

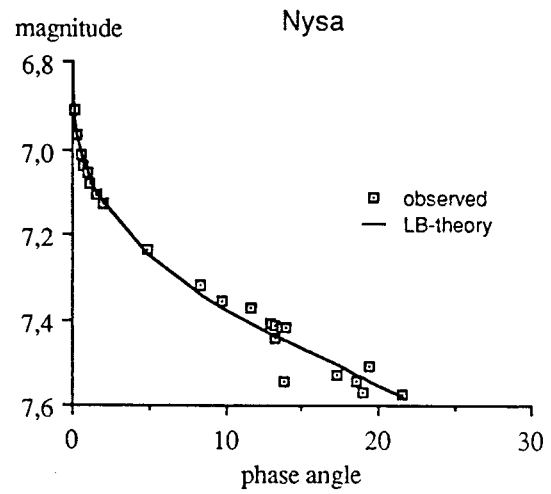
Nysa
magnitude
6,8
7,0
7,2
7,4
7,6
observed
LB-theory
0
10
20
30
phase angle

Fig. 6b

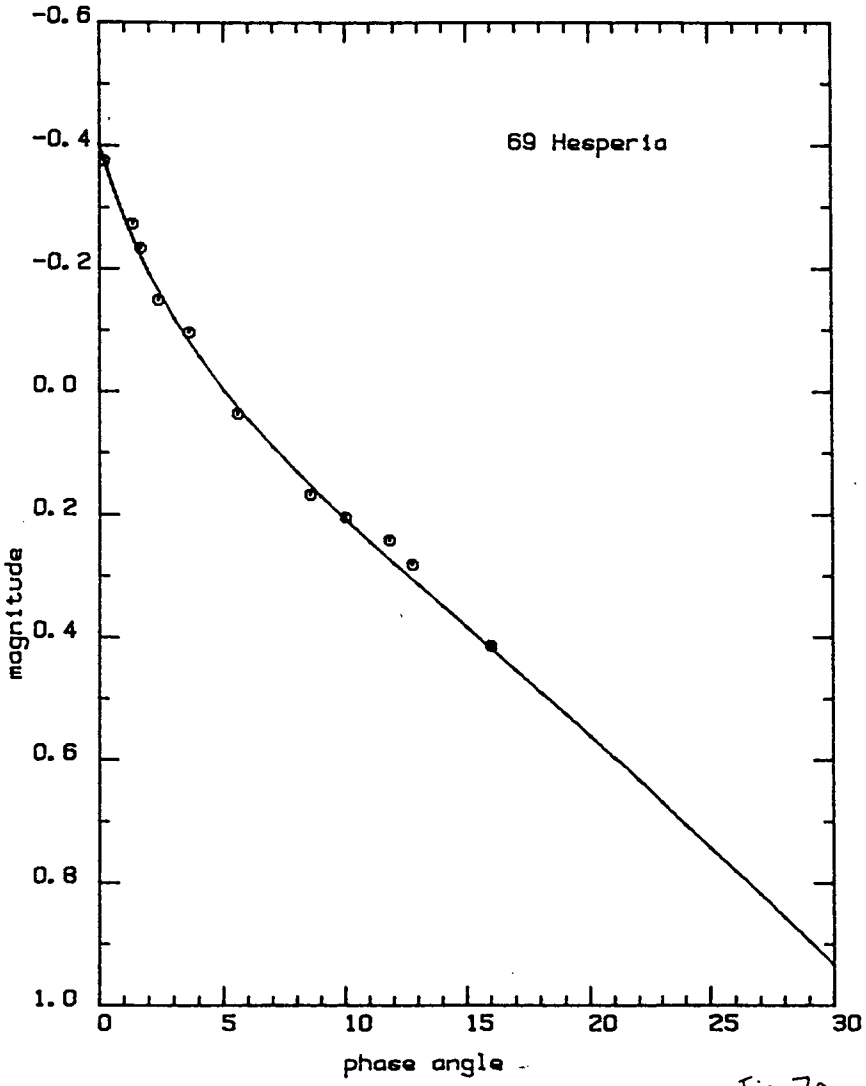
69 Hesperia
magnitude
phase angle
-0.6
-0.4
-0.2
0.0
0.2
0.4
0.6
0.8
1.0
0
5
10
15
20
25
30

Fig. 7a

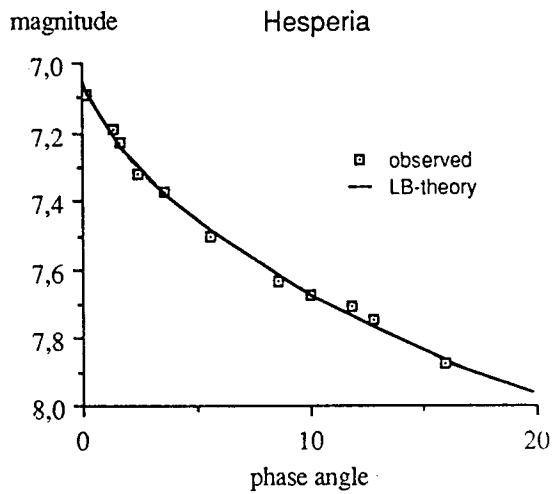
magnitude
Hesperia
observed
LB-theory
7,0
7,2
7,4
7,6
7,8
8,0
0
10
20
phase angle

Fig. 7b

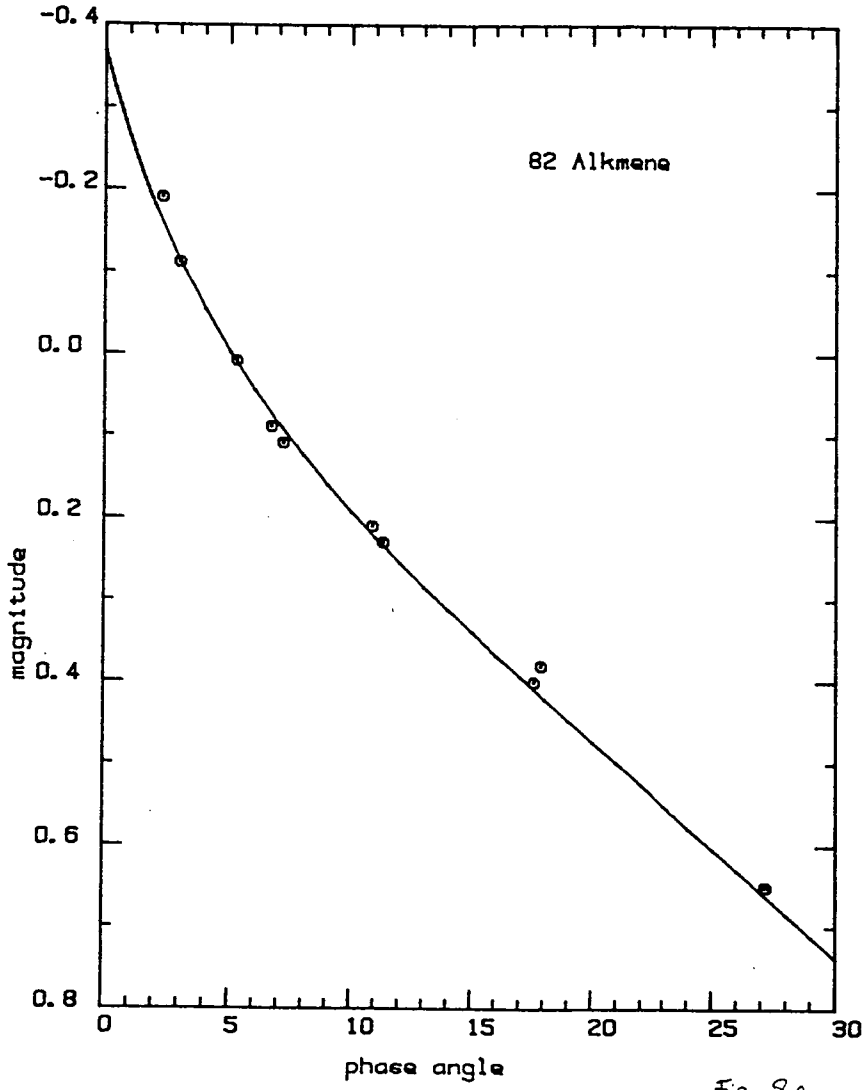
82 Alkmene
magnitude
phase angle
-0.4
-0.2
0.0
0.2
0.4
0.6
0.8
0
5
10
15
20
25
30

Fig. 8a

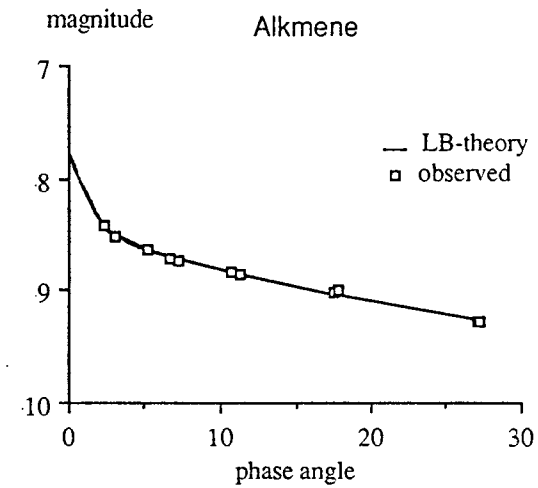
magnitude
Alkmene
LB-theory
observed
7
8
9
10
0
10
20
30
phase angle

Fig. 8b

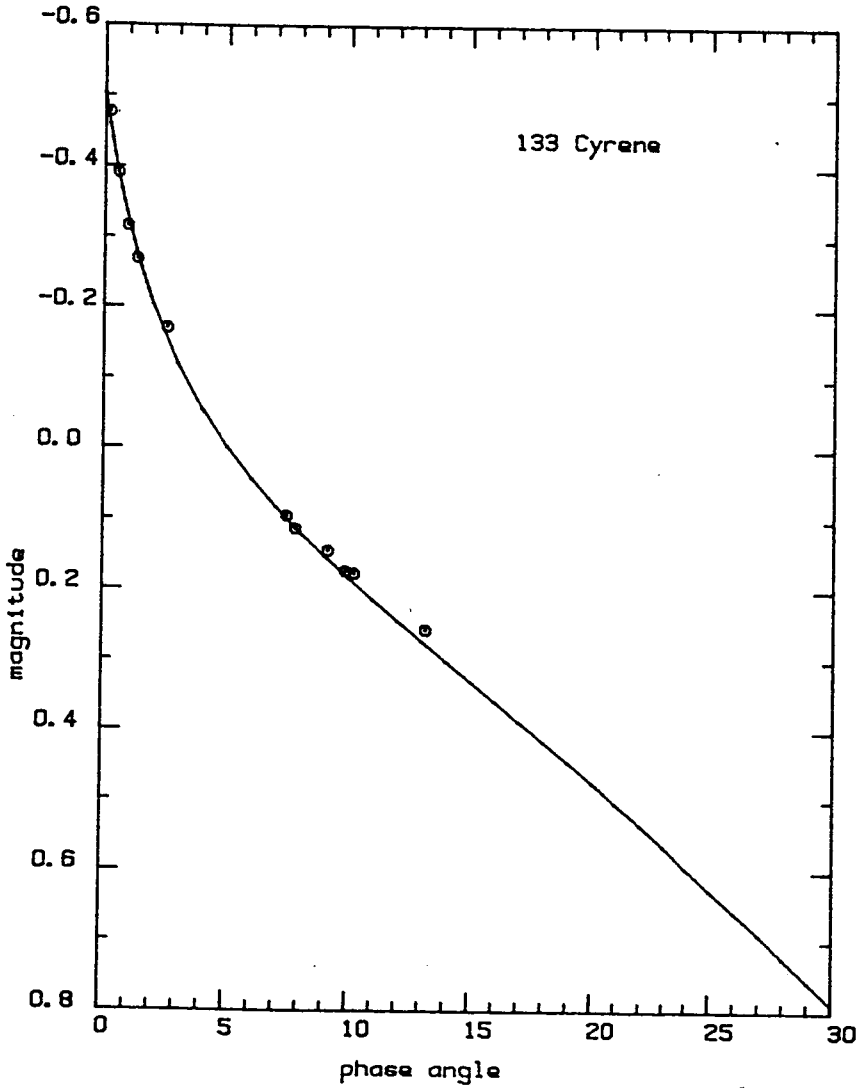
133 Cyrene
magnitude
phase angle
-0.6
-0.4
-0.2
0.0
0.2
0.4
0.6
0.8
0
5
10
15
20
25
30

Fig. 9a

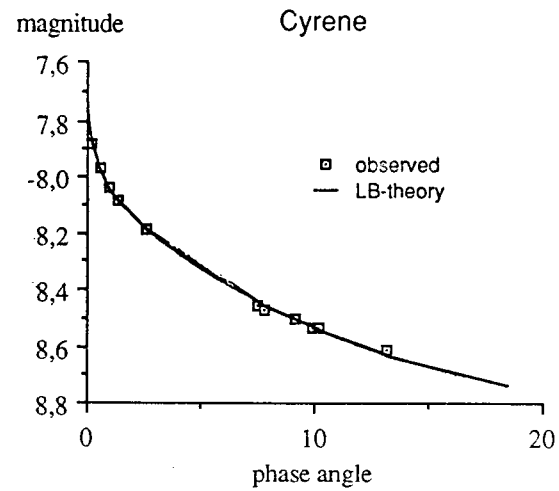
magnitude
Cyrene
observed
LB-theory
7,6
7,8
-8,0
8,2
8,4
8,6
8,8
0
10
20
phase angle

Fig. 9b

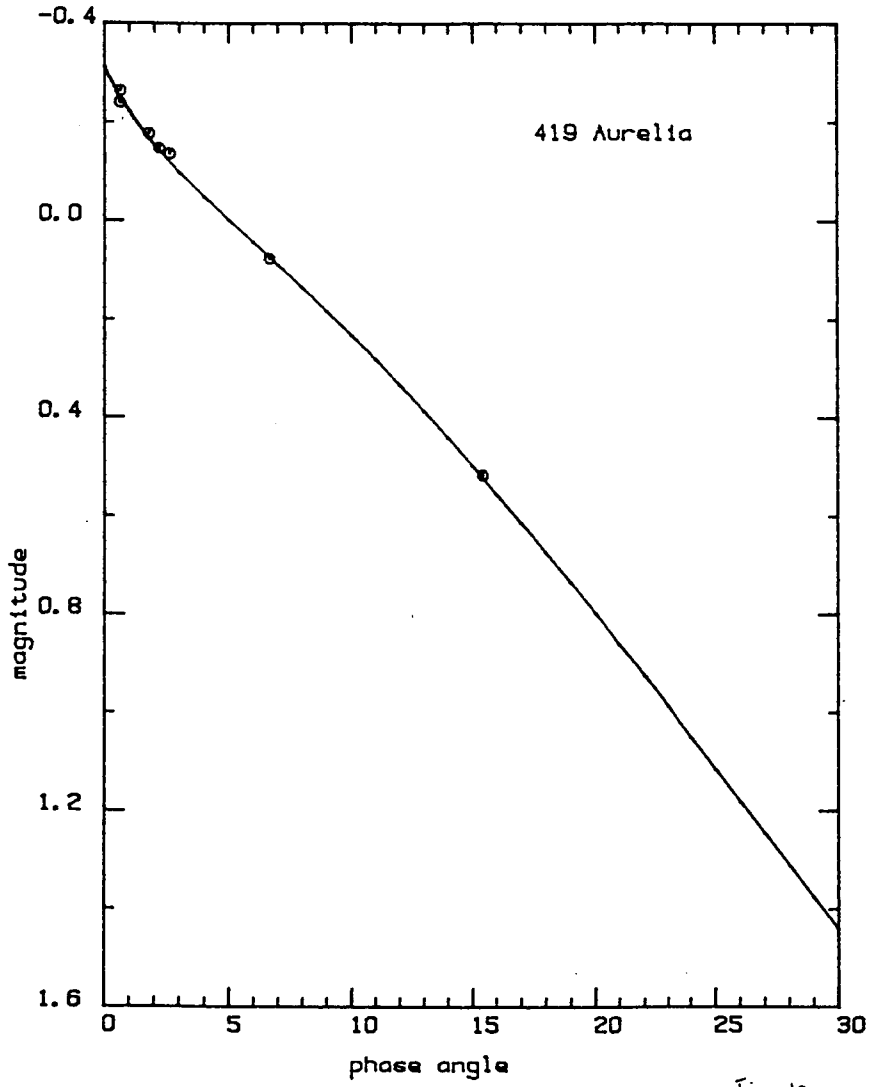

Fig. 10a

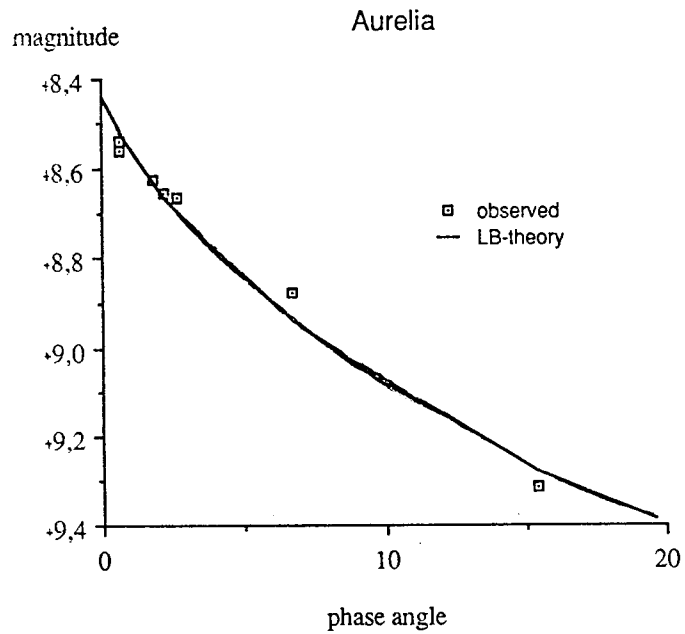

Fig. 10b

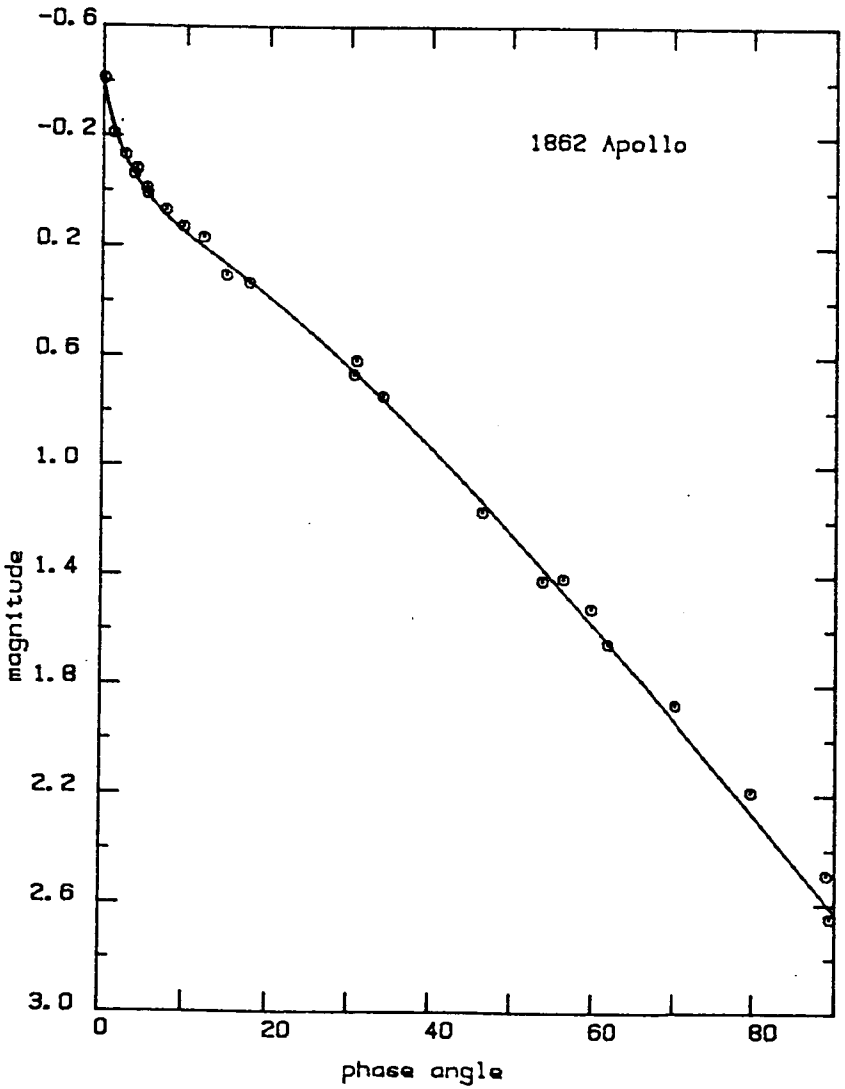

Fig. 11a

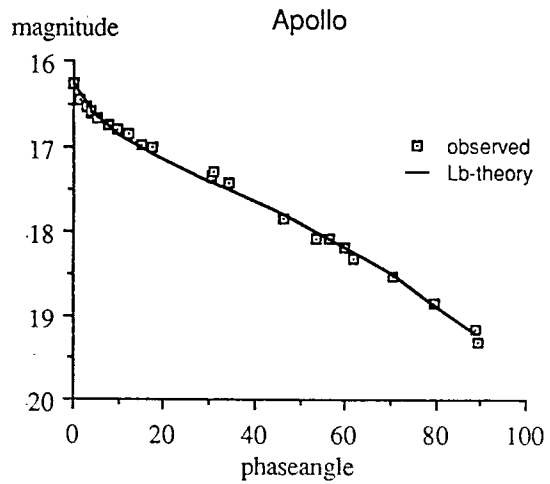

Fig. 11b